European Journal of Medicinal Chemistry 77 (2014) 110–120

Contents lists available at ScienceDirect

European Journal of Medicinal Chemistry

journal homepage: http://www.elsevier.com/locate/ejmech

Original article

Novel ruthenium complexes ligated with 4-anilinoquinazoline derivatives: Synthesis, characterisation and preliminary evaluation of biological activity

Liyun Ji [a,b,1], Wei Zheng [a,b,1], Yu Lin [a,b], Xiuli Wang [c], Shuang Lü [a,b], Xiang Hao [a,b], Qun Luo [a,b,*], Xianchan Li [a,b], Ling Yang [c], Fuyi Wang [a,b,*]

[a] Beijing National Laboratory for Molecular Sciences, PR China
[b] CAS Key Laboratory of Analytical Chemistry for Living Biosystems, Institute of Chemistry, Chinese Academy of Sciences, Beijing 100190, PR China
[c] Laboratory of Pharmaceutical Resource Discovery, Dalian Institute of Chemical Physics, Chinese Academy of Sciences, Dalian 116023, PR China

ARTICLE INFO

Article history:
Received 28 August 2013
Received in revised form
24 February 2014
Accepted 28 February 2014
Available online 1 March 2014

Keywords:
Ruthenium complexes
EGFR inhibitors
Multi-targeting
Anticancer agents
MCF-7

ABSTRACT

The ruthenium DMSO complexes *cis*-$Ru^{II}C1_2(DMSO)_4$ and $[(DMSO)_2H][trans\text{-}Ru^{III}Cl_4(DMSO)_2]$ reacted with 4-(3′-chloro-4′-fluoroanilino)-6-(2-(2-aminoethyl)aminoethoxy)-7-methoxyquinazoline (L1), 4-(3′-chloro-4′-fluoroanilino)-6-(2-(1H-imidazol-1-yl)ethoxy)-7-methoxy quinazoline (L2), N-(benzo[*d*]imidazol-4-yl)-6,7-dimethoxyquinazolin-4-amine hydrochloride (L3), 5-(6,7-dimethoxyquinazolin-4-ylamino)quinolin-8-ol hydrochloride (L4), respectively, to afford $[Ru^{II}Cl_2(DMSO)_2(L1)]$ (**1**), $[Ru^{III}Cl_3(DMSO)(L1)]$ (**2**), $[Ru^{III}Cl_4(DMSO)(H\text{-}L2)]$ (**3**), $[Ru^{III}Cl_4(DMSO)(H\text{-}L3)]$ (**4**), and $[Ru^{III}Cl_3(DMSO)(H\text{-}L4)]$ (**5**), which were characterised by mass spectrometry, NMR, elementary analysis and single crystal X-ray diffraction (complex **1**). Experimental screening (ELISA) showed that complexes **1**, **2** and **3** are remarkably inhibitory towards epidermal growth factor receptor (EGFR) with IC_{50} values at submicromolar or nanomolar level. Docking studies indicated that complexation with ruthenium has little interference with the formation of the two essential H-bonds between the N3 of the quinazoline ring in L1 and L2 and O–H of Thr766 through a water molecule, and the N1 of the quinazoline ring and N–H of Met769 in EGFR. Moreover, complex **2** was shown to be more active against the EGF-stimulated proliferation of human breast cancer cell line MCF-7 than the better EGFR inhibitor 4-(3′-chloro-4′-fluoroanilino)-6,7-dimethoxyquinazoline, being more potential to induce early-stage apoptosis than gefitinib. These imply that apart from inhibiting EGFR, complex **2** may involve in regulating other biological events related to the proliferation of MCF-7, implicating a novel type of multi-targeting metal-based anticancer agents.

1. Introduction

Since the serendipitous discovery of the biological activity of cisplatin in 1965 [1] and its subsequent clinical use for the treatment of various solid tumours including genitourinary, colorectal, and non-small cell lung cancers [2], medicinal inorganic chemistry has become a subject of intensive studies and continues to attract much attention in the drug discovery field [3,4]. However, the clinical use of cisplatin is largely restricted by dose-limiting side-effects such as neuro-, hepato- and nephrotoxicity, and inherent or acquired resistance [2,3]. During the past three decades, therefore, continuous effort has been devoted to the development of new platinum drugs and other metal-based, in particular ruthenium-based anticancer drugs to circumvent these limitations [3–8].

Current interest in ruthenium anticancer complexes was stimulated by the discovery of $(H_2im)[trans\text{-}RuCl_4(Him)(DMSO)]$ (NAMI-A, Him = imidazole) [9,10] and Indazolium *trans*-[tetrachlorobis(1*H*-indazole)ruthenate(III)] (KP1019) [11], of which both are being in clinic trails. NAMI-A is *in vivo* active to prevent the development and growth of pulmonary metastases in all the solid tumours [6,9]. KP1019 can induce apoptosis at non-toxic levels *via* the mitochondrial pathway and exhibits promising activity against certain types of tumours which are not successfully treatable with cisplatin [11,12].

* Corresponding authors. CAS Key Laboratory of Analytical Chemistry for Living Biosystems, Institute of Chemistry, Chinese Academy of Sciences, No. 2 the First North Street, Zhongguancun, Beijing 100190, PR China.
E-mail addresses: quoluo@iccas.ac.cn (Q. Luo), fuyi.wang@iccas.ac.cn (F. Wang).
[1] These authors contributed equally to this work.

http://dx.doi.org/10.1016/j.ejmech.2014.02.062
0223-5234/

Another reason that ruthenium attracts increasing attention in drug discovery field is that the well known octahedral ruthenium centre provides many synthetic opportunities for controlling and tuning the biological activities of inorganic pharmaceuticals by organising a wide range of multi-functional ligands in the three-dimensional space [3,13–19]. On the one hand, subject to extra-/intracellular hydrolysis or reduction, either Ru^{II} or Ru^{III} centre itself in these ruthenium complexes is the main reactive site towards biological molecules as has been reported for Ru^{II} in the ruthenium arene complexes [(η^6-arene)Ru(YZ)(X)][PF_6] [20–22], where X is a halide, YZ a chelating diamine such as ethylenediamine (en), and for Ru^{III} in KP1019 [12,23]. On the other hand, ruthenium has been used as a scaffold to organise various well-established bioactive organic pharmacophores around the metal centre [14,16]. In these cases, the Ru centre is either active [24–28] or solely a building block but not involved in any direct interactions with biological targets [29,30]. For example, coordinating with a potential leaving group (chloride), the Ru centre in ruthenium arene complexes bearing protein kinase inhibiting tyrphostin or topoisomerase inhibiting flavonoid moieties are active towards DNA while the bioactive ligands show inhibitory potential towards epidermal growth factor receptor (EGFR) and topoisomerase, respectively [24,27], which conferring the target complexes with dual- or multi-functional potential. However, in a series of organometallic ruthenium complexes mimicing the three dimensional structure of staurosporine [14,29–31], a highly potent protein kinase inhibitor (PKI), the ruthenium centre is inert while the entire molecules show highly inhibitory potency towards protein kinases such as Pim-1 [32] and glycogen synthase kinase 3β (GSK3β) [30].

Recently, we have synthesised a series of EGFR inhibiting 4-anilinoquinazoline derivatives [33] which can be linked to organometallic ruthenium fragments, affording novel dual-functional ruthenium complexes [34]. The complexation with organoruthenium fragments confers the 4-anilinoquinazoline pharmacophores higher potential inducing cellular apoptosis while the highly inhibitory activity of 4-anilinoquinazolines against EGFR and the reactivity of the ruthenium centre to 9-ethylguanine well preserve [34]. In the present work, we have designed and synthesised a series of Ru^{II}/Ru^{III} DMSO complexes bearing 4-anilinoquinazoline derivatives, which are analogues of gefitinib, a specific inhibitor of EGFR for clinic treatment of locally advanced or metastatic non-small cell lung cancer (NSCLC) [35]. Our goal is conferring the ruthenium complexes inhibitory potency against EGFR while maintaining the original activity, for instance cytotoxicity, of the ruthenium pharmacophores as much as possible.

2. Results and discussion

2.1. Chemistry

To develop a suitable ligand containing the 4-anilinoquinazoline pharmacophore for coordination to either Ru^{II} or Ru^{III}, very recently, we have synthesised a series of 4-anilinoquinazoline derivatives by modifying the pharmacophore using various substituents at either the 6- or 4-position of quinazoline core (Scheme 1) [33]. The precursor compound 4-(3′-chloro-4′-fluoro)-6-hydroxy-7-methoxyquinazoline reacted with 1, 2-dibromoethane in the presence of potassium carbonate at 353 K, giving rise to the modified 4-anilinoquinazoline intermediate 4-(3′-chloro-4′-fluoroanilino)-6-(2-bromoethoxy)-7-methoxyquinazoline (L′), and then L′ reacted with ethylenediamine (en) and imidazole (Im) in acetonitrile at 353 K to form 4-anilinoquinazoline derivatives L1

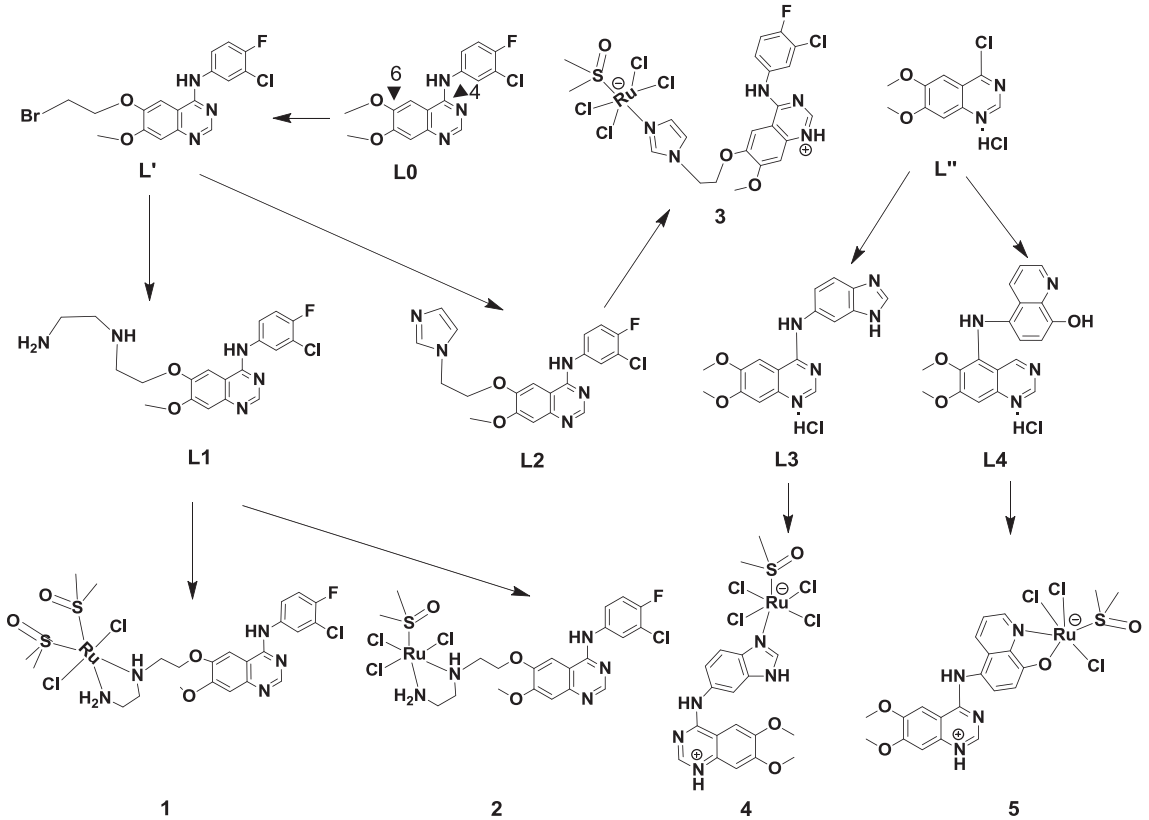

Scheme 1. Synthesis and Chemical structures of 4-anilinoquinazoline derivatives and Ru(II) (**1**) and Ru(III) (**2**, **3**, **4** and **5**) complexes containing 4-anilinoquinazoline derivatives and DMSO ligands.

and L2, respectively (Scheme 1). The reactions of the precursor compound 4-chloro-6,7-dimethoxyquinazoline (L′′) with 5-aminobenzoimidazole and 5-aminoquinolin-8-ol gave rise to 4-anilinoquinazoline derivatives L3 and L4, respectively [33], as shown in Scheme 1.

The reactions between the 4-anilinoquinazoline derivative L1 with the ruthenium-DMSO complexes *cis*-$Ru^{II}C1_2(DMSO)_4$ and $[(DMSO)_2H][trans\text{-}Ru^{III}Cl_4(DMSO)_2]$ afforded complexes $[Ru^{II}Cl_2(DMSO)_2(L1)]$ (**1**) and $[Ru^{III}Cl_3(DMSO)(L1)]$ (**2**), respectively. Slow diffusion of diethyl ether into the DMSO/acetone (1:5) solution of **1** gave rise to yellow plate crystals suitable for X-ray diffraction analysis. The X-ray structure and atom numbering scheme are shown in Fig. 1, crystallographic data and the selected bond lengths and angles are listed in Tables 1 and 2. It can be seen that the coordination sphere around the ruthenium centre constitutes a distorted octahedron with coordination of the bidentate (N–N) ligand L1, and two chloride ions in a *trans*-configuration and two DMSO through the S atom in a *cis*-configuration. The Ru–S bond distance for the two DMSO ligand are 2.2474(18) and 2.2557(18) Å, and the S–O bond lengths are 1.483(6) and 1.499(5) Å, respectively. The S–O bond lengths are shorter than that in free DMSO molecule (1.531(5) Å) [36], indicating a considerable increase of double-bond character of the S–O bond upon coordination to ruthenium *via* the sulphur atom. The bonds between Ru(II) ion and the N–N bidentate ligand (2.120(6) and 2.182(5)Å, respectively) are similar to those found in Ru(II) complexes containing polypyridine ligand [37], but slightly longer than those in the ruthenium(II) phosphine/diimine/picolinate complexes [38].

The reactions of Ru(III) complex $[(DMSO)_2H][trans\text{-}Ru^{III}Cl_4(DMSO)_2]$ with 4-anilinoquinazoline derivatives L2, L3 and L4 afforded complexes **3**, **4** and **5**, respectively (Scheme 1). In the 4-anilinoquinazoline derivative L3, the hydrogen atom can be located on either of the two nitrogen atoms in the benzoimidazole moiety. Thus L3 exists in two non-equivalent tautomeric forms, of which both can coordinate to ruthenium *via* the non-protonated N. Indeed, our LC-MS analysis shows that complex **4** presents in a pair of tautomeric forms as evidenced by identical mass spectra (data not shown) and different HPLC retention time (Fig. 2a).

Fig. 2 shows the HPLC chromatograms (Fig. 2a) of the five ruthenium complexes in DMSO as well as the UV–Vis spectra recorded during the HPLC analysis (Fig. 2b). It can be seen that (i) there is little hydrolysis reaction occurring during the HPLC separation; and (ii) apart from the absorption bands corresponding to the aromatic rings of the 4-anilinoquinazoline ligands, these complexes show strong ligand-to-metal charge transfer (LMCT) absorption centred at 342 nm with a shoulder band at ca. 400 nm upon the coordination of ruthenium (II or III) with the ligands. Complex **5** bearing the bidentate (N–, O–) ligand L4 exhibits the weakest LMCT absorption at 342 nm but the strongest absorption at 400 nm. The LMCT absorption bands of these ruthenium complexes

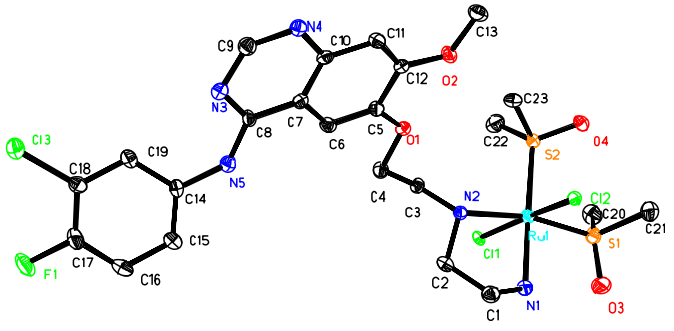

Fig. 1. X-ray crystal structure and atom numbering scheme for $[Ru^{II}Cl_2(DMSO)_2(L1)]$ (**1**) at 50% probability thermal ellipsoids.

Table 1
Crystallographic data of complex **1**.

Formula	$C_{23}H_{33}C_{13}FN_5O_4RuS_2$
Molecular weight	734.08
Crystal system	Triclinic
Space group	P-1
a (Å)	12.5570(17)
b (Å)	14.3849(17)
c (Å)	18.7823(19)
β(°)	93.090(7)
V (Å^3)	3091.7(6)
Z	4
Crystal size (mm)	0.20 × 0.13 × 0.07
Crystal description	plate
Crystal colour	yellow
D_x (Mg m^{-3})	1.577
μ (mm^{-1})	0.945
T (K)	173(2)
Wavelength (Å)	0.71073 (Mo-Kα)
Data-collection mode	ω scans
θ_{max} (°)	27.48
No. of integrated refl.	34,682
R_{int}	0.0507
Final *R* and R_w	0.0821, 0.2301
No. of parameters	723
$\Delta\rho_{max}$, $\Delta\rho_{min}$ (e Å^{-3})	3.084, −1.109

containing 4-anilinoquinazoline ligands slightly shift to visible light region and the absorption signals increase in intensity, especially at 350 nm, compared to those of the Ru^{II} arene complex [(η^6-biphenyl)Ru(ethylenediamine)Cl]$^+$ [39] and the Ru^{III} complex Na[*trans*-$RuCl_4$(indazole)$_2$] [40].

In view of the potential importance of aquation in the biological mechanism of action of the ruthenium complexes **1**–**5** as reported to the ruthenium(II) arene complexes [17,39,41–43] and ruthenium(III) complexes such as NAMI-A and KP1019 [40,44–47], complex **2** was chosen for a preliminary hydrolysis study. As shown in Fig. 3, apart from the HPLC peak corresponding to the intact complex **2**, there are two new HPLC peaks observed for the solution of complex **2** in the mixture of DMSO/H_2O (1:9, v/v) incubated at 310 K for 30 min. The intact species decreased and the new species b and c, which were identified by LC–MS to be L1 (*m/z* 406.2 for the most abundant isotopomer of $[M + H]^+$) and the hydrolytic product $[Ru^{III}Cl_2(DMSO)(L1)(H_2O)]^+$ (**2a**, *m/z* 655.6 for $[M - H_2O]^+$), increased in content with increase in incubation time. Although there was no HPLC peak detected and corresponding to the hydrolytic product $[Ru^{III}Cl_3(DMSO)(H_2O)]^+$ (**2b**) formed by dissociation of complex **2** because this highly polar species may has no

Table 2
Selected bond lengths (Å), angles and torsion (°) for complex **1**.

Ru(1)-N(1)	2.120(6)	Ru(1)-N(2)	2.182(5)
Ru(1)-S(1)	2.2474(18)	Ru(1)-S(2)	2.2557(18)
Ru(1)-Cl(1)	2.4670(14)	Ru(1)-Cl(2)	2.4497(14)
S(1)-O(3)	1.483(6)	S(2)-O(4)	1.499(5)
O(1)-C(4)	1.454(7)	O(2)-C(13)	1.432(8)
C(1)-C(2)	1.499(10)	C(3)-C(4)	1.511(9)
N(1)-C(1)	1.501(9)	N(2)-C(2)	1.497(8)
S(1)-Ru(1)-Cl(1)	90.20(6)	S(1)-Ru(1)-N(1)	87.23(16)
S(1)-Ru(1)-Cl(2)	94.24(6)	S(1)-Ru(1)-N(2)	167.92(15)
S(2)-Ru(1)-Cl(1)	96.53(6)	S(2)-Ru(1)-N(1)	175.47(16)
S(2)-Ru(1)-Cl(2)	88.68(6)	S(2)-Ru(1)-N(2)	98.40(14)
N(1)-Ru(1)-Cl(1)	87.91(16)	N(1)-Ru(1)-N(2)	80.8(2)
N(1)-Ru(1)-Cl(2)	86.82.(16)	Cl(1)-Ru(1)-Cl(2)	172.94(5)
N(2)-Ru(1)-Cl(1)	87.64(14)	S(1)-Ru(1)-S(2)	93.64(7)
N(2)-Ru(1)-Cl(2)	86.88(14)	N(1)-C(1)-C(2)	106.5(6)
Ru(1)-N(1)-C(1)	109.5(4)	N(2)-C(2)-C(1)	110.0(6)
Ru(1)-N(2)-C(2)	107.1(4)	N(2)-C(3)-C(4)	113.0(5)
S(1)-Ru(1)-N(2)-C(2)	−3.1(10)	Cl(1)-Ru(1)-N(2)-C(2)	76.8(4)
S(2)-Ru(1)-N(2)-C(2)	173.0(4)	Cl(2)-Ru(1)-N(2)-C(2)	−98.8(4)

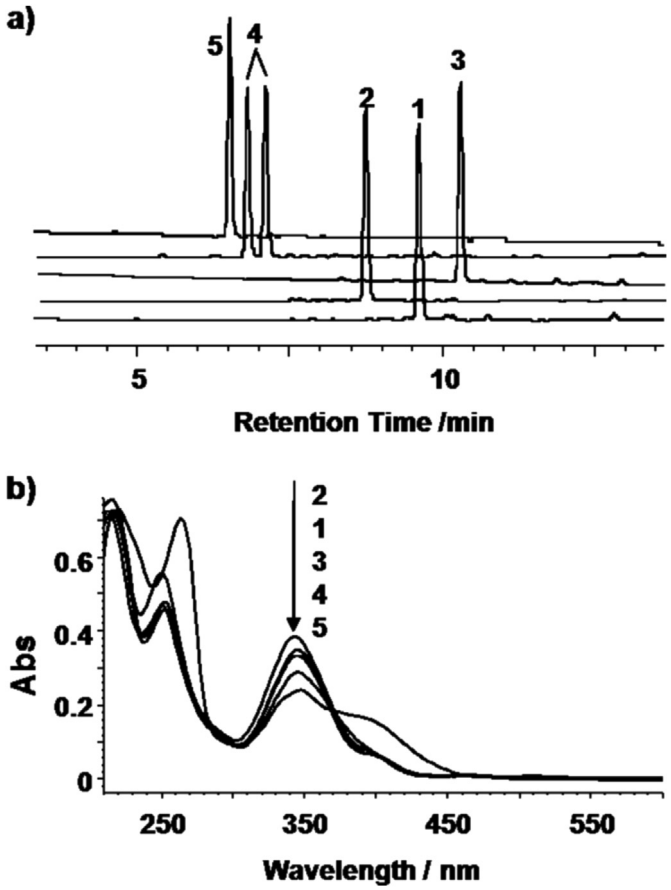

Fig. 2. (a) HPLC Chromatograms with UV detection at 350 nm of complexes **1**–**5** (1 mM) in DMSO; (b) UV–Vis spectra of complexes **1**–**5** recorded during the HPLC analysis, of which the chromatograms are shown in (a).

retention in the C18 reverse phase HPLC column, these results unambiguously indicate that complex **2** can be hydrolysed *via* the substitution of either the 4-anilinoquinazoline ligand (L1) or one of the chloride ligands. The HPLC time course (Fig. 3) indicate that the hydrolysis of complex **2** did not reach equilibrium status until 12 h, suggesting that the hydrolysis rate of complex **2** is much lower than those of [(η^6-biphenyl)Ru(ethylenediamine)Cl]$^+$ [39] and indazolium [trans-tetrachlorobis(1H-indazole)ruthenate(III)] (KP1019) [44], of which the half lives of hydrolysis under physiological relevant conditions are 9.02 and 17.1 min, respectively.

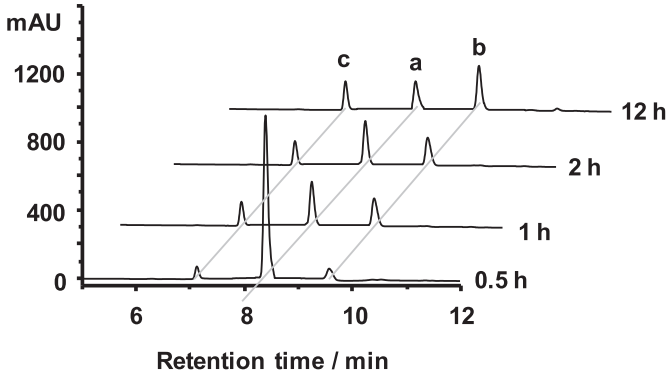

Fig. 3. HPLC time course with UV detection at 260 nm for the aquation of complex **2** (1 mM) in mixture of DMSO and H_2O (v/v: 1/9) incubated at 310 K. Peak assignment: a, intact complex **2** ([$Ru^{III}Cl_3$(DMSO)(L1)]); b, hydrolytic product [$Ru^{III}Cl_2$(DMSO)(L1)(H_2O)]$^+$; c, L1 dissociated from complex **2**.

2.2. Enzyme assays

We have previously determined the IC_{50} values, which are the concentration of the enzyme inhibitors requested to gain 50% inhibition against the targeted enzyme, of the 4-anilinoquinazoline derivatives L0–L4 (Scheme 1) against EGFR by enzyme-linked immunosorbent assay (ELISA) to be 3.8, 12.1, 60.2 nM, >5 μM and >5 μM, respectively [33]. These indicate that the substitution by N-containing groups ethylenediamine (en) and imidazole (Im) *via* the C2 alkyl linker at the 6-methoxyl position of the 4-anilinoquinazoline pharmacophore has no significant effect on its inhibition capacity against EGFR, but the modification on the aniline moiety remarkably reduces the inhibitory potency of 4-anilinoquinazoline pharmacophore as happened to L3 and L4 (Scheme 1).

Here, we applied the same method to characterise the inhibitory activity of the five ruthenium complexes bearing a 4-anilinoquinazoline ligand (Scheme 1) against EGFR. With the well-known EGFR inhibitor L0 [48] as a reference, at the dose of 10 μM, the relative inhibition efficiency (%) of the 4-anilinoquinazoline derivatives (L0–L4) and their ruthenium complexes **1**–**5** were measured to be 100 (L0), 100 (L1), 100 (L2), 77 (L3), 58 (L4), 99.95 (**1**), 98.56 (**2**), 98.47 (**3**), 23.8 (**4**) and 51 (**5**), respectively. These indicate that Ru(II) or Ru(III) coordination to the en in L1, Im in L2 or the quinoline group in L4 has no pronounced effect on the inhibitory activity of the respective 4-anilinoquinazoline derivatives towards EGFR. However, the Ru^{III} DMSO unit ligated with L3 through coordination with the nitrogen atom of benzoimidazole in L3 significantly reduces the inhibitory potency of L3.

Next, the IC_{50} values to EGFR of the active complexes **1**, **2** and **3** were determined, the concentration-dependent inhibitory curves are shown in Fig. 4 and IC_{50} values are listed in Table 3. The results indicate that Ru-coordination to en in L1 pronouncedly reduces the inhibitory activity of L1 towards EGFR, but the IC_{50} values of the resulting complexes **1** and **2** are still at sub-micromolar level. Notably, although the Im modification at the 6-position leads to a pronounced reduction of the inhibitory capacity of the 4-anilinoquinazoline pharmacophore, the activity of the 4-anilinoquinazoline derivative L2 against EGFR remain intact subject to the Ru(III) coordination to the Im group.

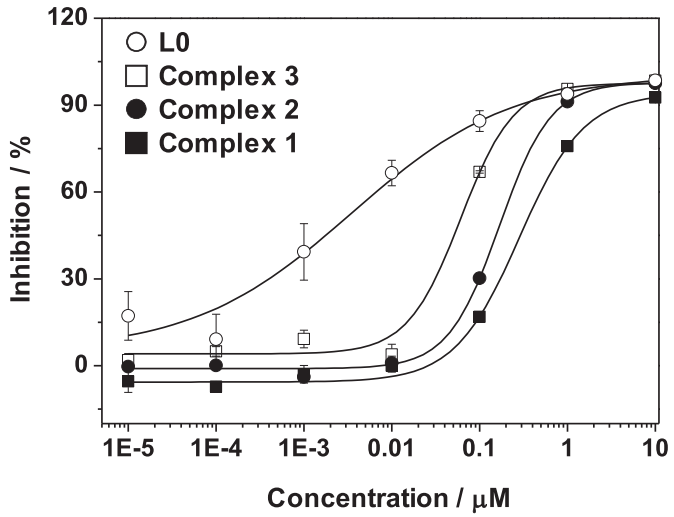

Fig. 4. Concentration–response inhibition curves of the 4-anilinoquinazoline derivatives L1 and L2 and the ruthenium complexes **1**, **2** and **3** on EGFR. *Points*: mean ± SD of triplicate determinations.

Table 3
IC_{50} for inhibition of EGFR and of the growth of MCF-7 cancer cells of ruthenium complexes **1**–**5**.

Compound	IC_{50} to EGFR/nM[a]	IC_{50} to MCF-7/μM[b]	
		− EGF	+ EGF
1	283 ± 11.0	>100	>100
2	168 ± 7.4	92.1 ± 2.2	18.3 ± 1.9
3	60.8 ± 3.5	>100	>100
4	>10 μM	>100	>100
5	>5 μM	>100	>100
L0	3.8 ± 2.5	>100	55.3 ± 3.1
RM116[c]	N. A.[d]	13.0 ± 3.4	21.8 ± 1.7

[a] The IC_{50} values were determined in the presence of 100 mM ATP.
[b] The cells were exposed with each tested compound for 48 h.
[c] RM116 = $[(\eta^6\text{-}p\text{-cym})Ru(en)Cl]PF_6$.
[d] Not applicable.

2.3. Docking analysis

We have previously established an indirect docking analysis method using the Surflex-Dock module of Sybyl X 1.1 program with introduction of the orders "-fmatch" and "-cpen" [33]. Herein, we applied this similar method to dock complexes **1**, **2** and **3** into the ATP-binding pocket in the EGFR kinase domain. It is worthy of pointing out that because the hydrolysis of these ruthenium complexes are slow (*supra vide*), the complexes were docked in their intact forms as shown in Scheme 1. Interestingly, although Ru(II) coordination to the bidentate en group leads to formation of an additional H-bond between the O at 7-postion of quinazoline ring and the amide N of Asp 776 (Fig. 5a), and Ru(III) coordination to the en group of L1 leads to formation of two additional H-bonds between the N–H of en and the COO^- of Asp 776, and the N–H of en and the backbone C–O of Leu694 (Fig. 5b), the ruthenium coordination reduces the inhibition capacity of L1 (Table 3). In contrast, without inducing formation of new H-bond between L2 and EGFR kinase domain (Fig. 5c), Ru(III) binding to the imidazole group of L2 has little impact on the inhibition activity of L2 against EGFR. One of possible explanation is that compared to the non-coordinated L1, the poses of ligand L1 of complexes **1** and **2** at the ATP binding cleft of EGFR are changed significantly due to Ru coordination (Fig. 5a, b). However, the Ru coordination to the Im group does not change the conformation of the ligand L2 of complex **3** at the ATP-binding cleft of EGFR (Fig. 5c).

2.4. Antiproliferation potency

To evaluate the anticancer potency of the EGFR inhibiting ruthenium complexes **1**–**3,** we employed sulforhodamine B (SRB) colourimetric assay to screen the *in vitro* antiproliferation activity of ruthenium complexes **1**, **2** and **3** towards human breast cancer cell line MCF-7, which has been reported to overexpress EGF receptor [49,50], in the absence and the presence of EGF. The well-established EGFR inhibitor L0 [48] and the cytotoxic ruthenium arene complex $[(\eta^6\text{-}p\text{-cym})Ru^{II}(en)Cl]PF_6$ (RM116) [51] were used as positive references during the *in vitro* screening. The dose-dependent inhibition curves of the tested compounds on the growth of MCF-7 are shown in Fig. 6, and the resulting IC_{50} values are listed in Table 3.

The results indicate that in the presence of 10 nM EGF, the EGFR inhibiting L0 exhibited dose-dependent inhibition on the proliferation of MCF-7 cancer cells, the average IC_{50} value from three experiments was 55.3 μM. While even at 100 μM, L0 showed little inhibition on the proliferation of MCF-7 in the absence of EGF. This implies that the 4-anilinoquinazoline derivative (L0) indeed exert its inhibition on proliferation of MCF-7 *via* blocking EGFR signalling

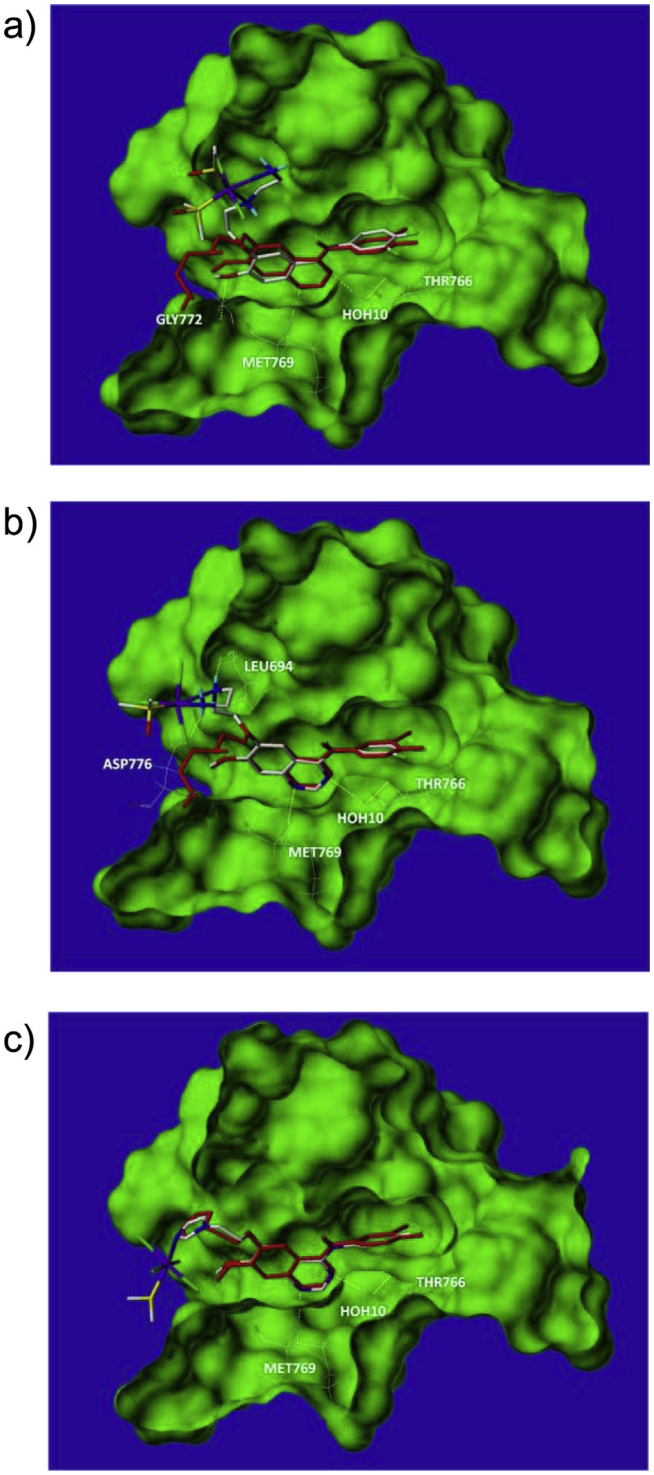

Fig. 5. The docked conformers/poses of complexes (a) **1**, (b) **2** and (c) **5** (coloured by atoms) and their 4-anilinoquinazoline ligands L1 (red, for **1** and **2**) and L2 (red, for **3**) at the ATP binding cleft of EGFR kinase as generated *via* Surflex docking-scoring combinations. The dotted yellow lines illustrate the positions of probable H-bonding interactions as calculated by the H-Bond calculator imbedded in the Surflex-Dock module of Sybyl X 1.0 program. (For interpretation of the references to colour in this figure legend, the reader is referred to the web version of this article.)

[35]. In contrast, the cytotoxic organometallic ruthenium complex RM116 exhibited EGF-independent inhibition on the proliferation of MCF-7, the IC_{50} values range from 13.0 to 21.8 μM, similar to that of RM119 against human ovarian cancer line A2780 [51].

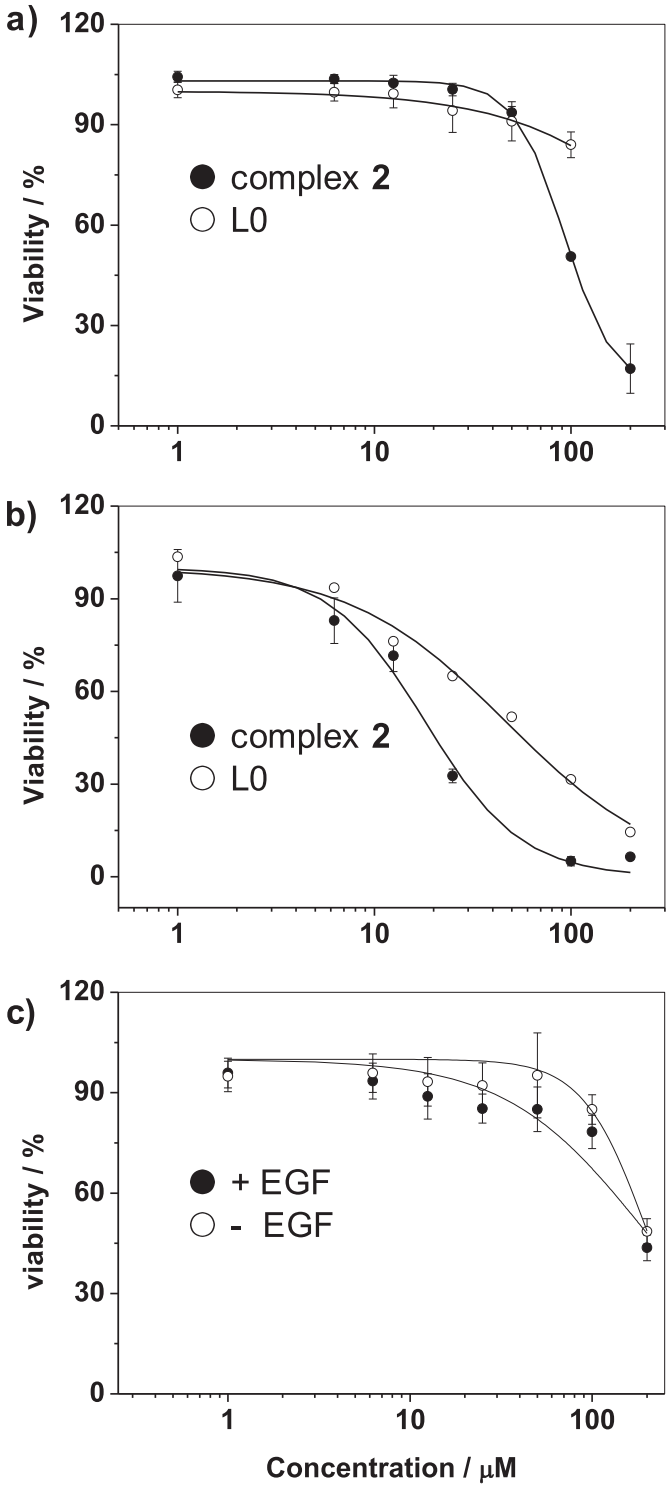

Fig. 6. (a, b) Dose-dependent inhibition curves of complex **2** and 4-anilinoquinazoline derivative L0 on the growth of human breast cancer cell line MCF-7 in the absence (a) and in the presence (b) of EGF (10 nM). (c) Dose-dependent inhibition curves of complex **2** on the growth of human embryonic kidney cell line HEK293 in the absence or in the presence of EGF (10 nM).

Interestingly, bearing the EGFR inhibiting 4-anilinoquinazoline L1 or L2 [33], ruthenium complexes **1**, **2** and **3** showed different antiproliferation activity on MCF-7. The Ru^{III} complex **2** ([$Ru^{III}Cl_3$(DMSO)(L1)]) exhibited a remarkably EGF-stimulation-dependent inhibition on proliferation of MCF-7, while complexes **1** and **3** are inactive towards the growth of MCF-7 cells. The inhibitory potency of complex **2** on the EGF-induced growth of MCF-7 is similar to that of the non-specific and cytotoxic organoruthenium complex RM116 [51] and pronouncedly higher than that of L0, though the inhibitory capacity of complex **2** on EGFR is lower than that of L0. These imply that other than blocking EGFR signalling, complex **2** may inhibit the proliferation of MCF-7 *via* other ways, for example inducing apoptosis *via* the mitochondrial pathway through hydrolytic activation as does KP1019 [11], or *via* blocking DNA synthesis and replication as supposed to cytotoxic ruthenium complex RM116 [52].

The cytotoxicity of complex **2** on the growth of the normal human embryonic kidney 293 (HEK293) cells was also tested. The dose-dependent inhibition curves are showed in Fig. 6c, corresponding to IC_{50} values being 195 ± 10 and 188 ± 18 μM in the absence and in the presence of EGF, respectively. These results further verify the highly selective inhibition of complex **2** on the EGF-induced growth of MCF-7 cancer cells.

2.5. Induction of apoptosis

In order to understand the mechanism of action of complex **2**, the capacity of complex **2** to induce apoptotic cell death was evaluated by fluorescence microscopy imaging of MCF-7 stained with 4,6-diamidino-2-phenylindole (DAPI). The monofunctional EGFR inhibitor gefitinib is thought to exert its effect by blocking the mitogen-activated protein kinase (MAPK) signalling pathway and to have less capacity to induce apoptotic cell death [53]. The ruthenium arene compound RM116 containing the cytotoxic pharmacophore (arene)Ru(en) is anticipated to be more active to induce apoptosis [51]. Indeed, the microscopic image (Fig. 7c) gives clear evidence of the formation of more apoptotic bodies, characterised by the fragmentation of nuclei with condensed chromatin, upon the treatment of MCF-7 with the cytotoxic RM116 than those resulting from the treatment with EGFR inhibiting gefitinib and complex **2** (Fig. 7b and d). Furthermore, the flow cytometric quantification indicated that complex **2** (Fig. 7h) induced more early-stage apoptosis and necrosis than gefitinib did (Fig. 7f), though the inhibitory potency of gefitinib (IC_{50} = 33 nM [54]) is higher than that of complex **2** (IC_{50} = 168 nM). These results suggest that (i) ligation with the EGFR inhibiting anilinoquinazoline derivative L1 makes the NAMI-like complex **2** *in vitro* cytotoxic towards primary cancer cell line MCF-7, and (ii) complexation with the Ru^{III}(DMSO) chlorido fragment confers the effective EGFR inhibitor L1 with additional capacity inducing cellular apoptosis, in particular early-stage apoptosis, to the blockade of MAPK signalling.

3. Conclusions

In conclusion, in this work, we demonstrate that the modification by ethylenediamine or imidazole group at 6-postion of the 4-anilinoquinazoline derivatives L0 allows this well-established pharmacophore to serve as a chelating or monodentate ligands of which the complexation with Ru^{II} and Ru^{III} DMSO fragments affords complexes to give rise to a new type of Ru complexes with interesting inhibitory potency against EGFR. Moreover, the Ru^{III} DMSO complex [$Ru^{III}Cl_3$(DMSO)(L1)] (**2**, L1 = 4-(3′-chloro-4′-fluoroanilino)-6-(2-(2-aminoethyl)-aminoethoxy)-7-methoxyqui nazoline) exhibits higher *in vitro* inhibitory potency specifically on the EGF-induced proliferation of cancer cell line MCF-7 than the non-coordinated 4-anilinoquinazoline derivative L0 (4-(3′-chloro-4′-fluoroanilino)-6,7-dimethoxyquinazoline) which is more active against EGFR than complex **2**. The apoptosis assays indicate that complex **2** is more active to induce early-stage apoptosis than gefitinib, a clinically used

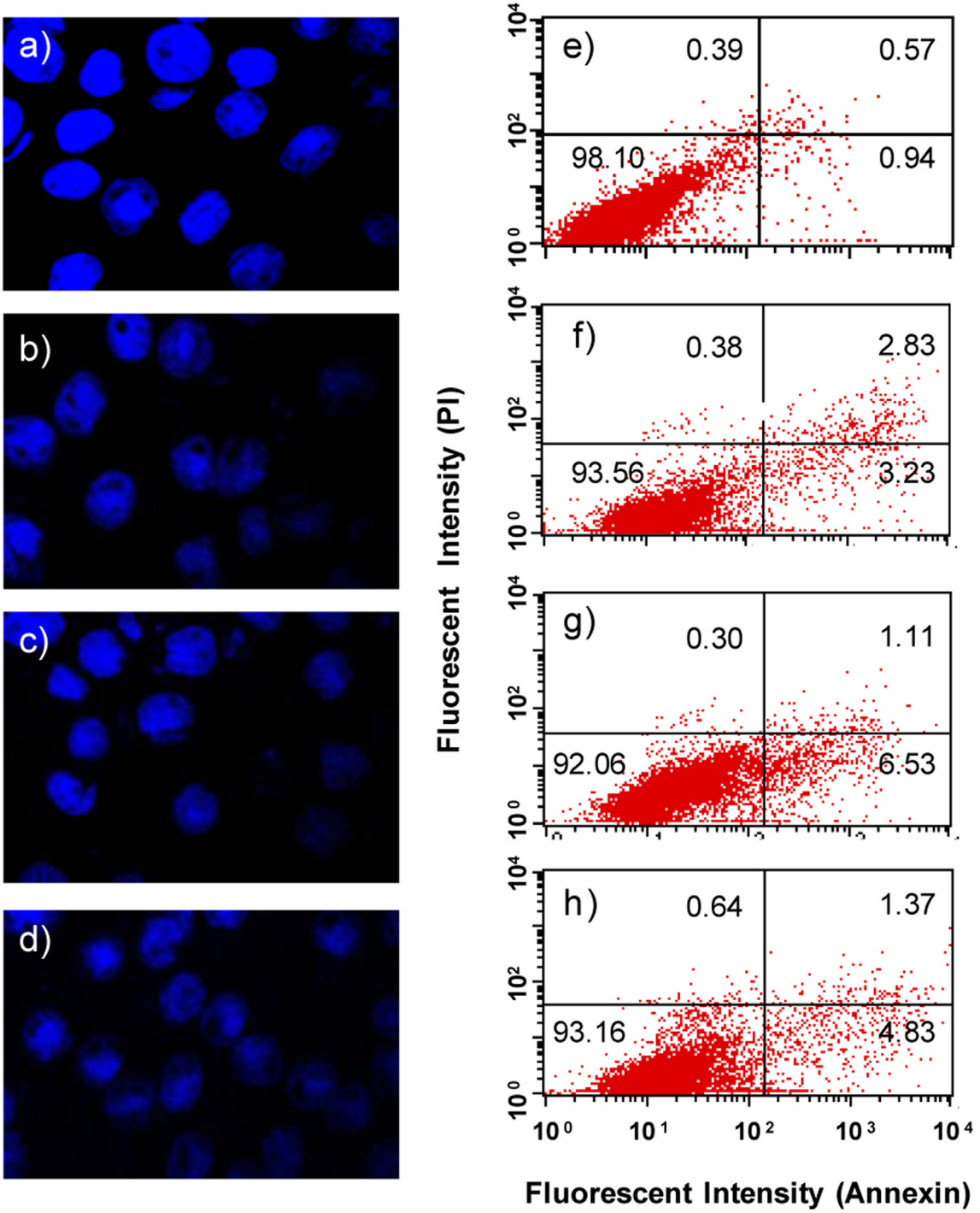

Fig. 7. Confocal fluorescent images (left) with emission at 461 nm and flow cytometric quantification (right) of viability (bottom left quadrant), early-stage apoptosis (bottom right quadrant), late-stage apoptosis (top right quadrant) and necrosis (top left quadrant) of MCF-7 cells treated with 50 μM of different compounds in the presence of 10 nM EGF at 310 K for 24 h. The number in each quadrant indicates the respective percentages of total cell populations. (a, e) untreated control; (b, f) gefitinib; (c, g) RM116; (d, h) complex **2**.

anticancer drug. These imply that complex **2** may exert inhibition on the proliferation of MCF-7 not only *via* blocking the EGFR signalling, but also *via* other pathways, for example, blocking DNA synthesis and replication. In other words, complex **2** may represent a novel class of multi-targeting anticancer agents involving both blockage of EGFR signalling and induction of early-stage apoptosis cascades. To this regard, it is worthy of further studies in details for elucidation of the molecular mechanism of action of complex **2**.

4. Experimental section

4.1. Materials

$RuCl_3 \cdot 3H_2O$ (Ru > 36.7%) was purchased from Shenyang Jingke Reagent Co. (China), the Catalyst Pd/C from Beijing Ouhe Technology Co. (China), 4-chloro-6,7-dimethoxylquinazoline (AR grade) from Shanghai FWD Chemicals Co. (China), 5-nitro-8-

hydroxylquinoline from Wuhan Kaitong Fine Chemicals Co. (China), and Imidazole from Tianjin Jinke Fine Chemical Research Institute (China). Organic solvents including absolute methanol, absolute ethanol, absolute ether, acetonitrile, dichloromethane and DMSO were all analytical grade and used directly without further purification.

Column chromatography silica gel was purchased from Qingdao Jiyida Silica Reagent Manufacture (China), and thin layer chromatography silica gel from Yantai Institute of Chemical Industry Research (China). Trifluoroacetic acid (TFA) was purchased from Sigma, chromatographic grade acetonitrile from Tedia Company (China).

The protein tyrosine kinase epidermal growth factor receptor (EGFR), and the epidermal growth factor (EGF) were purchased from Sigma, and other biological agents including the ELISA kits for EGFR inhibitor screening from Cell Signaling Technology Inc. (USA). Sodium silicate nonahydrate ($Na_2SiO_3 \cdot 9H_2O$), cetyltrimethylammonium bromide (CTAB), iron nitrate nonahydrate ($Fe(NO_3)_3 \cdot 9H_2O$), ethylene glycol, ammonium hexafluorotitanate ($(NH_4)_2TiF_6$), boric acid (H_3BO_3) were purchased from Shanghai General Chemical Reagent Manufacture (China). The deionised water used in the experiments was prepared by a Milli-Q system (Millipore, Milford, MA).

4.2. Synthesis of ruthenium complexes **1**–**5**

The ruthenium DMSO precursor complexes *cis*-$Ru^{II}C1_2(DMSO)_4$ and $[(DMSO)_2H][trans\text{-}Ru^{III}Cl_4(DMSO)_2]$ were synthesised following the procedures reported in the literature [55,56]. The 4-anilinoquinazoline derivatives L0–L4 (Scheme 1) were synthesised following the procedures described in our previous work [33].

4.2.1. $[Ru^{II}Cl_2(DMSO)_2(L1)]$ (**1**)

The 4-anilinoquinazoline derivative L1 (40.58 mg, 0.1 mmol) was added to *cis*-$Ru^{II}C1_2(DMSO)_4$ (48.5 mg, 0.1 mmol) in dry ethanol (10 mL), and the mixture was held at 385 K for 6 h. A good quantity of precipitate formed, and the precipitate was filtered off, washed with ethanol and ether, and dried in vacuum to give rise to $[Ru^{II}Cl_2(DMSO)_2(L1)]$ (**1**) (40 mg, yield: 55%). ESI-MS (positive): *m/z* 736.2 for $[M + H]^+$ (theoretical *m/z* 736.0). ^1H NMR (DMF-d_7) δ(ppm): 8.58 (s, 1H), 8.33 (d, 1H), 8.31 (d, 1H), 7.95–7.92 (m, 1H), 7.48–7.46 (m, 1H), 7.45–7.43 (m, 1H), 7.29 (m, 1H), 4.49 (2H, br s), 4.39 (1H, br s), 4.00 (s, 3H), 3.28–3.26 (m, 8H), 2.58 (s, 12H). ^{13}C NMR (DMF-d_7) δ (ppm): 157.1 (Ar-C), 155.7 (Ar-C), 153.6 (Ar-C), 149.2 (Ar-C), 148.4 (Ar-C), 138.1 (Ar-C), 123.9 (Ar-C), 122.6 (Ar-C), 119.9 (Ar-C), 117.1 (Ar-C), 117.0 (Ar-C), 109.9 (Ar-C), 108.2 (Ar-C), 103.8 (Ar-C), 68.6 (OCH_2), 57.3 (OCH_3), 56.4 ($NHCH_2$), 50.6 ($NHCH_2$), 46.1 (NH_2CH_2), 45.4 ($SOCH_3$), 44.8 ($SOCH_3$), 44.3 ($SOCH_3$), 43.6 ($SOCH_3$).

X-ray diffraction-quality crystals were grown by slow diffusion of diethyl ether into the DMSO/acetone (1:5) solutions of **1**.

4.2.2. $[Ru^{III}Cl_3(DMSO)(L1)]$ (**2**)

The 4-anilinoquinazoline derivative L1 (40.58 mg, 0.1 mmol) dissolved in 6 mL EtOH/MeCN, was added to $[(DMSO)_2H][trans\text{-}RuCl_4(DMSO)_2]$ (55.6 mg, 0.1 mmol) in dry ethanol (4 mL), and the mixture was stirred for 30 min at room temperature. Then 4 mL H_2O was added and the mixture was stirred for another 30 min. The yellow solid, appeared in the solution, was filtered off, washed with ethanol and diethyl ether, and dried in vacuum to afford $[Ru^{III}Cl_3(DMSO)(L1)]$ (**2**) (43 mg, yield: 62%). ESI-MS (positive): *m/z* 693.1 for $[M + H]^+$ (theoretical *m/z* 693.0). ^1H NMR (DMF-d_7) δ (ppm): −5.30 (very broad), −14.18 (very broad) for *S*-DMSO ligand. Anal. Calcd for $C_{21}H_{27}Cl_4FN_5O_3RuS \cdot 3H_2O$ (F.W.: 745.9): C, 33.83; H, 4.46; N, 9.39. Found: C, 33.80; H, 4.13; N, 9.18.

4.2.3. $[Ru^{III}Cl_4(DMSO)(H\text{-}L2)]$ (**3**)

Complex **3** was synthesised following a similar procedure reported in the literature [57,58]. The precursor complex $[(DMSO)_2H][trans\text{-}RuCl_4(DMSO)_2]$ (0.036 mmol) was dissolved in 4 mL of EtOH/HCl (0.1 M), the resulting solution was stirred for 5 min at room temperature, and 0.072 mmol of 4-anilinoquinazoline derivative L2 was then added. The orange solution was stirred for 24 h, and the yellow solid appeared in the solution was filtered off, washed with ethanol and diethyl ether, and dried in vacuum to give rise to complex **3** (10.6 mg, yield: 40%). ESI-MS (negative): *m/z* 735.2 for $[M - H]^-$ (theoretical *m/z* 734.9). ^1H NMR (DMF-d_7) δ (ppm): −13.09 (very broad) for *S*-DMSO ligand. Anal. Calcd for $C_{22}H_{24}Cl_5FN_5O_3RuS$ (F.W.: 735.9): C, 35.91; H, 3.29; N, 9.52. Foud: C, 35.88; H, 3.70; N, 8.93.

4.2.4. $[Ru^{III}Cl_4(DMSO)(H\text{-}3)]$ (**4**)

This complex was prepared following a procedure similar to that for synthesis of complex **3**. The precursor complex $[(DMSO)_2H][trans\text{-}RuCl_4(DMSO)_2]$ (0.036 mmol) was dissolved in 4 mL of EtOH/HCl (0.1 M). The resulting solution was stirred for 5 min at room temperature and 0.072 mmol of 4-anilinoquinazoline derivative L3 was then added. The orange solution was stirred for 24 h, and the yellow solid appeared in the solution was filtered off, washed with ethanol and diethyl ether, and dried in vacuum to give rise to complex **4** (10 mg, yield: 43%). ESI-MS (negative): *m/z* 643.1 for $[M - H]^-$ (theoretical *m/z* 642.9). ^1H NMR (DMF-d_7) δ (ppm): −13.17 (very broad) for *S*-DMSO ligand. Anal. Calcd for $C_{19}H_{22}Cl_4N_5O_3RuS \cdot H_2O$ (F.W.: 661.9): C, 34.50; H, 3.66; N, 10.59. Found: C, 34.11; H, 3.81; N, 10.13. IR (cm^{-1}): 3452w, br, 1635vs, 1573m, 1512vs, 1437m, 1409m, 1280m, 1221m, 1065s, 1022s, 852m.

4.2.5. $[Ru^{III}Cl_3(DMSO)(H\text{-}L4)]$ (**5**)

The precursor complex $Na[trans\text{-}RuCl_4(DMSO)_2]$ (0.036 mmol) was dissolved in absolute methanol (4 mL). The resulting solution was stirred for 5 min at room temperature, and the 4-anilinoquinazoline derivative L4 (0.036 mmol) in methanol was then added. The resulting solution was stirred for 6 h, and the precipitate appeared in the solution was filtered off, washed with methanol and diethyl ether, and dried in vacuum to afford complex **5** (49% yield). ESI-MS (negative): *m/z* 634.1 for $[M - H]^-$ (theoretical *m/z* 633.9). ^1H NMR (DMF-d_7) δ (ppm): −6.38 (broad), −8.36 (very broad) for *S*-DMSO ligand. Anal. Calcd for $C_{21}H_{22}Cl_3N_4O_4RuS \cdot 2H_2O$ (F.W.: 670.9): C, 37.65; H, 3.91; N, 8.36. Found: C, 38.27; H, 4.43; N, 7.70. IR (cm^{-1}): 3446w, br, 3066m, 3005m, 2941m, 2844m, 2634s, 1583s, 1512s, 1463m, 1436m, 1409m, 1381m, 1365m, 1309m, 1296m, 1279m, 1228s, 1071m, 1022s.

It is notable that the NMR characterisation of complexes **2**–**5** was not informative due to the paramagnetic effect of the Ru^{III} ions. However, one or two broadened ^{1}signals of the two $-CH_3$ groups in the DMSO ligand of these complexes are distinguished, significantly moving towards high field, and can be indicative of the presence of asymmetric methyl groups in complexes **2** and **5** and symmetric methyl groups in complexes **3** and **4**.

4.3. X-ray crystallography

Single-crystal X-ray diffraction study for $[Ru^{II}Cl_2(DMSO)_2(L1)]$ (**1**) was carried out using graphite monochromated MoKα radiation ($\lambda = 0.71073$ Å) on a Rigaku Saturn 724 CCD area detector. All data were collected at 173 K, and structure solution and refinement were performed using the SHELXL-97. Standard data relating to the X-ray crystal structure of complex **1** have been deposited in the

Cambridge Crystallographic Data Centre with the CCDC deposition number CCDC866471.

4.4. High performance liquid chromatography (HPLC)

An Agilent 1200 series quaternary pump and a Rheodyne sample injector with a 20-μL loop, an Agilent 1200 series UV–Vis DAD detector and Chemstation data processing system were used to separate the hydrolytic mixtures of complex **2**. The HPLC analysis was carried out on an Agilent Eclipse XDB-C18 reversed-phase column (150 × 4.6 mm, 5 μM, USA). The mobile phases were water containing 0.1% TFA (solvent A), and acetonitrile containing 0.1% TFA (solvent B). The gradient at 1.0 mL min^{-1} was as follows: 10% solvent B to 80% from 0 to 20 min, 80% from 20 to 22 min, then resetting to 10% at 23 min.

4.5. Electrospray ionization mass spectrometry (ESI-MS)

Negative- or positive-ion ESI mass spectra were obtained on a Micromass Q-TOF spectrometer (Waters) equipped with a Masslynx (ver. 4.0) data processing system for analysis and post processing. For the online LC-ESI-MS assays, an Agilent 1200 system was interfaced with the mass spectrometer, using the same column and gradients as described above for the HPLC assays with a flow rate of 1 mL/min and a splitting ratio of 1/10 into mass spectrometer. The spray voltage and the cone voltage were 2.8–3.8 kV and 55–70 V, respectively. The desolvation temperature was 393 K and the source temperature 373 K. Nitrogen was used as both cone gas and desolvation gas with a flow rate of 50 L h^{-1} and 500 L h^{-1}, respectively. The collision energy was set up to 10 V. The spectra were acquired in the range of 200–1200 *m/z*. The mass accuracy of all measurements was within 0.1 *m/z* unit, and all *m/z* values are the mass-to-charge ratios of the most abundant isotopomer for observed ions.

4.6. Elemental analysis and NMR spectroscopy

Elemental analysis was carried out on a Flash EA 1112 element analysis instrument (ThermoQuest). ^1H NMR spectra were obtained on a Bruker Avance 400 spectrometer (Germany).

4.7. Hydrolysis

The stock solution of complex **2** (8 mM) was prepared by dissolving the complex in DMSO. To initial the hydrolysis of complex **2**, 10 μL DMSO solution of complex **2** was mixed with 90 μL, and the resulting mixture was incubated at 310 K. Then HPLC data were recorded at four time intervals, 0.5, 1, 2 and 12 h. And the products generated from the hydrolysis were identified by LC-ESI-MS.

4.8. Kinase inhibition assay

Enzyme-linked immunosorbent assay (ELISA) was applied to characterise the inhibition potency of ruthenium complexes **1**–**5** against EGFR. An aliquot (10 μL) of the enzyme solution was added to 415 μL DTT kinase buffer which is consist of 5 μL DTT (1.25 M) and 1.25 mL 4 × HTScan® Tyrosine Kinase Buffer (240 mM HEPES pH 7.5, 20 mM $MgCl_2$, 20 mM $MnCl_2$, 12 μM Na_3VO_4). Each tested complex was dissolved in dimethylsulphoxide (DMSO) to give a 4 mM solution which was diluted with 0.05% Tween-20 in deionised water to give a 40 μM solution.

The ATP/peptide mixture was prepared by addition of 10 μL of 10 mM ATP to 125 μL of 6 μM substrate peptide, and then diluted with D_2O to 250 μL. An aliquot (12.5 μL) of solution of a screened complex was mixed with as-prepared EGFR solution (12.5 μL) and incubated at room temperature for 5 min, followed by addition of 25 μL of ATP/substrate mixture, and then the resulting mixture was incubated at 310 K for 1 h. The phosphorylation reaction was terminated by the addition of 50 μL/well stop buffer (50 mM EDTA, pH 8).

Each well of a microtitre plate was coated with 100 μL of 10 μg mL^{-1} streptavidin in carbonate–bicarbonate buffer and incubated overnight at 277 K, and then blocked with 1.5% bovine serum albumin (BSA) in PBS/T (PBS solution contain 0.05% Tween-20) at 310 K for 2 h, followed by three times of washing with PBS/T prior to use. Then, aliquot (25 μL/well) of each enzymatic reaction mixture and 75 μL/well of D_2O were added to the wells (in triplicate) for incubation at 310 K for 1 h. Following three times of washing with PBS/T, 100 μL of primary antibody (Phospho-Tyrosine Mouse mAb, 1:1000 in PBS/T with 1.5% BSA) was added to each well and the plate was incubated at 310 K for another 1 h. The plate was again washed three times with PBS/T, and then 100 μL of secondary antibody (HRP-labelled Goat Anti-Mouse lgG, 1:1000 in PBS/T with 1.5% BSA) was added to each well for 1 h of incubation at 310 K, followed by three times of washing with PBS/T. Finally, 100 μL of TMB substrate system was added to each well and the plate was incubated at 310 K for 15 min, and the reaction was stopped by addition of 100 μL of 2 M H_2SO_4, and the plate was read on the ELISA plate reader (SpectraMax M5 Molecular Devices Corporation).

4.9. Docking analysis

The docking analysis was performed, a fully automatic docking tool available, running on Dual-core Intel(R) E5300 CPU 2.60 GHz, RAM Memory 2 GB under the Windows XP system. The crystal structure of the EGFR-erlotinib complex was collected from PDB under code 1M17 [59]. All the hydrogen atoms were added to define the correct configuration and tautomeric states. Then the modelled structure was energy-minimised using AMBER7FF99 force field with distance dependent dielectric function and current charges. The Powell energy minimisation algorithm was used for the energy minimisation. After extracting the binding ligand erlotinib, the structure corresponding to the constringent energy gradient (0.05 kcal mol^{-1}) was used for re-docking and scoring calculations of erlotinib to check the accuracy of the Surflex-Dock program. The 4-anilinoquinazoline-type analogues were then separately docked into the binding pocket for docking-scoring analysis.

4.10. In vitro antiproliferation assays

The human breast cancer cell line MCF-7 was obtained from the Centre for Cell Resource of Shanghai Institute for Biological Sciences, Chinese Academy of Science. MCF-7 cells were maintained in RPMI 1640 (Invitrogen, USA) media supplemented with 10% foetal calf serum (HyClone, USA). On requested, an aliquot of 100 ng mL^{-1} epidermal growth factor (Sigma, USA) was added into the media. The cells were grown at 310 K in a humidified atmosphere containing 5% CO_2 for 2–3 days prior to screening experiments.

The IC_{50} values, this is the concentration of tested compounds that inhibit 50% of cell growth of MCF-7 cell line were determined using the sulforhodamine B (SRB) technique. Cells were plated at a density of 6500 cells/well in 150 μL media in 96-well plates and grew in the absence or the presence of EGF for 24 h. The stock solutions (2 or 4 mM) of all tested complexes were made up fresh in 10% DMSO and saline before diluted down in media to give the required concentration for addition to the cells. The final concentration of DMSO in media was 0.5%. Cells were then exposed to each tested complex at various concentrations for 48 h and cell growth measured using SRB assay following the procedure reported by

Skehan et al. [60] Briefly, after 48 h exposure to the tested compounds, cells were fixed with 50 μL of cold trichloroacetic acid (50%) per well (96-well plate) for 60 min at 310 K. After washed five times with tap water, the cells were stained for 30 min at 298 K with 0.5% acetic acid containing 0.4% SRB (Sigma). Then, each plate was rinsed five times with 1% acetic acid and allowed to air dry. The resulting coloured residue was dissolved in 200 μL of Tris base (10 mM) and optical density (OD) value for each well was measured using a microplate reader (SpectraMax M5 Molecular Devices Corporation) at the wavelength of 570 nm. The inhibition rate (IR) was calculated based on the equation as follow:

$$IR(\%) = \left[1 - \left(OD_{compound} - OD_{blank}\right) \Big/ \left(OD_{control} - OD_{blank}\right)\right] \times 100\%$$

All reported values were averages of three independent experiments and expressed as mean ± SD (standard deviation).

The human embryonic kidney 293 cells (HEK293) was gifted by Professor Dihua Shangguan at the Institute of Chemistry, Chinese Academy of Science. The IC_{50} values of complex **2** on the growth of HEK293 in the absence and in the presence of EGF were measured by the analogical method described above.

4.11. Fluorescence microscopy

Induction of apoptosis in human breast cancer cell line MCF-7 was evaluated by confocal microscope after DAPI (4′, 6-diamidino-2-phenylindole) staining. Briefly, 1×10^5 cells per well were seeded on cover glasses in a 24-well plate and allowed to attach for 16 h at 310 K. Cells were then treated with the tested compounds at 310 K for 24 h. After removing the supernatant and washing the cells with PBS three times, the cells were fixed with the pre-cool methanol for 15 min. After that, the cells were treated with 1 μg mL^{-1} DAPI (Sigma) in deionised water in dark. Washing the cells with PBS, the cover glasses were then mounted on microscopy slides with glycerol. Fluorescence images were obtained on a Carl Zeiss LSM 510 META confocal microscope (Oberkochen, Germany) at excitation wavelength of 790 nm and emission wavelength of 461 nm.

4.12. Annexin v/propidium iodide (PI) double staining assay

To further verify the induction of apoptosis by the synthesised ruthenium complexes, MCF-7 cells were seeded in a density of 2×10^5 per well in a 6-well plate and allowed to attach for 16 h, then the cells were exposed to each tested compounds, including complex **2** and references, at 310 K for 24 h. The supernatant was removed, and cells were detached by trypsinization after washing by PBS. The cells were transferred to FACS tubes after washing by PBS and centrifuged at 1000 rpm for 3 min. After re-suspension in 0.5 mL binding buffer, the cells were incubated with 5 μL Annexin-V conjugate for 5 min, followed by addition of 5 μL PI prior to the FACS analysis. The FACS assays were preformed on a Calibur flow cytometer (BD, Franklin Lakes, New Jersey, US), of which the FL1 channel was used to record the intensity of annexin V-FITC staining and FL2 channel to record the intensity of PI staining. The data were quantified by Sell Quest software (BD, Franklin Lakes, New Jersey, US).

Acknowledgement

We thank NSFC (Grant Nos: 21020102039, 21135006, 21127901, 21275148 (Q. L.) and 21321003), the 973 Program of MOST (2013CB531805) for financial support.

Appendix A. Supplementary data

Supplementary data related to this article can be found at http://dx.doi.org/10.1016/j.ejmech.2014.02.062.

References

[1] B. Rosenber, L. Vancamp, T. Krigas, Nature 205 (1965) 698–699.
[2] Y.W. Jung, S.J. Lippard, Chemical Reviews 107 (2007) 1387–1407.
[3] P.C.A. Bruijnincx, P.J. Sadler, Current Opinion in Chemical Biology 12 (2008) 197–206.
[4] L. Kelland, Nature Reviews Cancer 7 (2007) 573–584.
[5] P.C.A. Bruijnincx, P.J. Sadler, Advances in Inorganic Chemistry 61 (2009) 1–62.
[6] P.J. Dyson, G. Sava, Dalton Transactions (2006) 1929–1933.
[7] T.W. Hambley, Dalton Transactions (2007) 4929–4937.
[8] A. Levina, A. Mitra, P.A. Lay, Metallomics 1 (2009) 458–470.
[9] E. Alessio, G. Mestroni, A. Bergamo, G. Sava, Current Topics in Medicinal Chemistry 4 (2004) 1525–1535.
[10] A. Bergamo, B. Gava, E. Alessio, G. Mestroni, B. Serli, M. Cocchietto, S. Zorzet, G. Sava, International Journal of Oncology 21 (2002) 1331–1338.
[11] C.G. Hartinger, S. Zorbas-Seifried, M.A. Jakupec, B. Kynast, H. Zorbas, B.K. Keppler, Journal of Inorganic Biochemistry 100 (2006) 891–904.
[12] M.A. Jakupec, M. Galanski, V.B. Arion, C.G. Hartinger, B.K. Keppler, Dalton Transactions (2008) 183–194.
[13] C.G. Hartinger, P.J. Dyson, Chemical Society Reviews 38 (2009) 391–401.
[14] E. Meggers, Current Opinion in Chemical Biology 11 (2007) 287–292.
[15] E. Meggers, G.E. Atilla-Gokcumen, H. Bregman, J. Maksimoska, S.P. Mulcahy, N. Pagano, D.S. Williams, Synlett (2007) 1177–1189.
[16] T. Storr, K.H. Thompson, C. Orvig, Chemical Society Reviews 35 (2006) 534–544.
[17] F.Y. Wang, A. Habtemariam, E.P.L. van der Geer, R. Fernandez, M. Melchart, R.J. Deeth, R. Aird, S. Guichard, F.P.A. Fabbiani, P. Lozano-Casal, I.D.H. Oswald, D.I. Jodrell, S. Parsons, P.J. Sadler, Proceedings of the National Academy of Sciences of the United States of America 102 (2005) 18269–18274.
[18] P. Sathyadevi, P. Krishnamoorthy, N.S.P. Bhuvanesh, P. Kalaiselvi, V.V. Padma, N. Dharmaraj, European Journal of Medicinal Chemistry 55 (2012) 420–431.
[19] H.J. Yu, Y. Chen, L. Yu, Z.F. Hao, L.H. Zhou, European Journal of Medicinal Chemistry 55 (2012) 146–154.
[20] H.M. Chen, J.A. Parkinson, R.E. Morris, P.J. Sadler, Journal of the American Chemical Society 125 (2003) 173–186.
[21] H.K. Liu, S.J. Berners-Price, F.Y. Wang, J.A. Parkinson, J.J. Xu, J. Bella, P.J. Sadler, Angewandte Chemie International Edition 45 (2006) 8153–8156.
[22] F.Y. Wang, J.J. Xu, A. Habtemariam, J. Bella, P.J. Sadler, Journal of the American Chemical Society 127 (2005) 17734–17743.
[23] F. Kratz, M. Hartmann, B. Keppler, L. Messori, Journal of Biological Chemistry 269 (1994) 2581–2588.
[24] B. Biersack, M. Zoldakova, K. Effenberger, R. Schobert, European Journal of Medicinal Chemistry 45 (2010) 1972–1975.
[25] A. Castonguay, C. Doucet, M. Juhas, D. Maysinger, Journal of Medicinal Chemistry 55 (2012) 8799–8806.
[26] W. Ginzinger, G. Muhlgassner, V.B. Arion, M.A. Jakupec, A. Roller, M. Galanski, M. Reithofer, W. Berger, B.K. Keppler, Journal of Medicinal Chemistry 55 (2012) 3398–3413.
[27] A. Kurzwernhart, W. Kandioller, C. Bartel, S. Bachler, R. Trondl, G. Muhlgassner, M.A. Jakupec, V.B. Arion, D. Marko, B.K. Keppler, C.G. Hartinger, Chemical Communications 48 (2012) 4839–4841.
[28] X.Y. Wei, L. Qi, G.L. Yang, F.Y. Wang, Talanta 79 (2009) 739–745.
[29] H. Bregman, P.J. Carroll, E. Meggers, Journal of the American Chemical Society 128 (2006) 877–884.
[30] H. Bregman, D.S. Williams, G.E. Atilla, P.J. Carroll, E. Meggers, Journal of the American Chemical Society 126 (2004) 13594–13595.
[31] E. Meggers, Angewandte Chemie International Edition 50 (2011) 2442–2448.
[32] J.E. Debreczeni, A.N. Bullock, G.E. Atilla, D.S. Williams, H. Bregman, S. Knapp, E. Meggers, Angewandte Chemie International Edition 45 (2006) 1580–1585.
[33] S. Lü, W. Zheng, L.Y. Ji, Q. Luo, X. Hao, X.C. Li, F.Y. Wang, European Journal of Medicinal Chemistry 61 (2013) 84–94.
[34] W. Zheng, Q. Luo, Y. Lin, Y. Zhao, X.L. Wang, Z.F. Du, X. Hao, Y. Yang, S. Lü, L.Y. Ji, X.C. Li, L. Yang, F.Y. Wang, Chemical Communications (2013), http://dx.doi.org/10.1039/c1033cc43000f.
[35] J. Baselga, Science 312 (2006) 1175–1178.
[36] M. Calligaris, O. Carugo, Coordination Chemistry Reviews 153 (1996) 83–154.
[37] J.G. Liu, Q.L. Zhang, X.F. Shi, L.N. Ji, Inorganic Chemistry 40 (2001) 5045–5050.
[38] F.R. Pavan, G.V. Poelhsitz, M.I.F. Barbosa, S.R.A. Leite, A.A. Batista, J. Ellena, L.S. Sato, S.G. Franzblau, V. Moreno, D. Gambino, C.Q.F. Leite, European Journal of Medicinal Chemistry 46 (2011) 5099–5107.
[39] F. Wang, H.M. Chen, S. Parsons, L.D.H. Oswald, J.E. Davidson, P.J. Sadler, Chemistry – A European Journal 9 (2003) 5810–5820.
[40] B. Cebrian-Losantos, E. Reisner, C.R. Kowol, A. Roller, S. Shova, V.B. Arion, B.K. Keppler, Inorganic Chemistry 47 (2008) 6513–6523.
[41] I. Berger, M. Hanif, A.A. Nazarov, C.G. Hartinger, R.O. John, M.L. Kuznetsov, M. Groessl, F. Schmitt, O. Zava, F. Biba, V.B. Arion, M. Galanski, M.A. Jakupec, L. Juillerat-Jeanneret, P.J. Dyson, B.K. Keppler, Chemistry – A European Journal 14 (2008) 9046–9057.

[42] C. Gossens, A. Dorcier, P.J. Dyson, U. Rothlisberger, Organometallics 26 (2007) 3969–3975.
[43] A.F.A. Peacock, A. Habtemariam, R. Fernandez, V. Walland, F.P.A. Fabbiani, S. Parsons, R.E. Aird, D.I. Jodrell, P.J. Sadler, Journal of the American Chemical Society 128 (2006) 1739–1748.
[44] M. Groessl, C.G. Hartinger, P.J. Dyson, B.K. Keppler, Journal of Inorganic Biochemistry 102 (2008) 1060–1065.
[45] A.V. Vargiu, A. Robertazzi, A. Magistrato, P. Ruggerone, P. Carloni, The Journal of Physical Chemistry B 112 (2008) 4401–4409.
[46] A.H. Velders, A. Bergamo, E. Alessio, E. Zangrando, J.G. Haasnoot, C. Casarsa, M. Cocchietto, S. Zorzet, G. Sava, Journal of Medicinal Chemistry 47 (2004) 1110–1121.
[47] M. Bacac, A.C.G. Hotze, K. van der Schilden, J.G. Haasnoot, S. Pacor, E. Alessio, G. Sava, J. Reedijk, Journal of Inorganic Biochemistry 98 (2004) 402–412.
[48] K.H. Gibson, W. Grundy, A.A. Godfrey, J.R. Woodburn, S.E. Ashton, B.J. Curry, L. Scarlett, A.J. Barker, D.S. Brown, Bioorganic & Medicinal Chemistry Letters 7 (1997) 2723–2728.
[49] M. Ono, A. Hirata, T. Kometani, M. Miyagawa, S. Ueda, H. Kinoshita, T. Fujii, M. Kuwano, Molecular Cancer Therapeutics 3 (2004) 465–472.
[50] K.B. Reddy, G.L. Mangold, A.K. Tandon, T. Yoneda, G.R. Mundy, A. Zilberstein, C.K. Osborne, Cancer Research 52 (1992) 3636–3641.
[51] R.E. Aird, J. Cummings, A.A. Ritchie, M. Muir, R.E. Morris, H. Chen, P.J. Sadler, D.I. Jodrell, British Journal of Cancer 86 (2002) 1652–1657.
[52] O. Novakova, J. Kasparkova, V. Bursova, C. Hofr, M. Vojtiskova, H.M. Chen, P.J. Sadler, V. Brabec, Chemistry & Biology 12 (2005) 121–129.
[53] M. Muhsin, J. Graham, P. Kirkpatrick, Nature Reviews Drug Discovery 2 (2003) 515–516.
[54] A.E. Wakeling, S.P. Guy, J.R. Woodburn, S.E. Ashton, B.J. Curry, A.J. Barker, K.H. Gibson, Cancer Research 62 (2002) 5749–5754.
[55] E. Alessio, G. Balducci, M. Calligaris, G. Costa, W.M. Attia, G. Mestroni, Inorganic Chemistry 30 (1991) 609–618.
[56] I.P. Evans, A. Spencer, G. Wilkinson, Journal of the Chemical Society Dalton Transactions (1973) 204–209.
[57] J.J. Fiol, A. Garcia-Raso, F.M. Alberti, A. Tasada, M. Barcelo-Oliver, A. Terron, M.J. Prieto, V. Moreno, E. Molins, Polyhedron 27 (2008) 2851–2858.
[58] A. Garcia-Raso, J.J. Fiol, A. Tasada, M.J. Prieto, V. Moreno, I. Mata, E. Molins, T. Bunic, A. Golobic, I. Turel, Inorganic Chemistry Communications 8 (2005) 800–804.
[59] J. Stamos, M.X. Sliwkowski, C. Eigenbrot, Journal of Biological Chemistry 277 (2002) 46265–46272.
[60] P. Skehan, R. Storeng, D. Scudiero, A. Monks, J. Mcmahon, D. Vistica, J.T. Warren, H. Bokesch, S. Kenney, M.R. Boyd, Journal of the National Cancer Institute 82 (1990) 1107–1112.